Using quantum memory techniques for optical detection of ultrasound

D. L. McAuslan, L. R. Taylor, and J. J. Longdell[a)]
Jack Dodd Centre for Photonics and Ultra-Cold Atoms, Department of Physics, University of Otago, Dunedin, New Zealand

(Received 17 July 2012; accepted 22 October 2012; published online 8 November 2012)

Quantum memories are inherently highly efficient and display low noise, making them particularly suitable for the optical detection of ultrasound. Here, we use an atomic-frequency-comb based quantum memory to demonstrate sensitive ultrasound detection, realising a 49 dB discrimination between the sidebands and the carrier. The method remains valid in the case of optically thin samples and thus represents a significant improvement over other ultrasound detection methods based on rare-earth-ion-doped crystals. Furthermore, we show that this non-destructive non-contact approach is also compatible with highly scattering samples and suggest its particular suitability for the real-time imaging of biological tissues. © *2012 American Institute of Physics*. [http://dx.doi.org/10.1063/1.4766341]

Ultrasound-modulated optical tomography (UOT) is a technique combining light and ultrasound for the imaging of soft-tissue biological systems, often used for early cancer detection.[1] While being very sensitive, optical imaging techniques are highly scattering in biological tissues, limiting the penetration depth. Ultrasound imaging is less sensitive than optical detection but has the ability to image deep into tissue without significant scattering. A combination of these two techniques would be desirable for highly sensitive, deeply penetrating imaging.

There are two main points to consider when using the UOT technique. First, the ultrasound frequency is typically eight orders of magnitude smaller than the optical frequency which can make detection difficult. Techniques based on interferometers[2] and optical cavities[3] can easily resolve such small frequency shifts; however, these techniques run into the problem of having a small etendue—which is the second consideration. The optical etendue of a detector is the product of its collection area and acceptance solid angle. To detect the scattered light that results from imaging biological samples, a large etendue is necessary.

One method allowing detection of ultrasound modulated photons with high etendue and high sensitivity uses photorefractive crystals (PRCs).[4–6] However, this technique has the disadvantage of being relatively slow, to the point of becoming impractical for use with living biological tissue: the typical response time of a PRC based system is 10–100 ms.[7,8] In contrast, the decorrelation time in biological tissue is less than 0.1 ms.[9]

Recently, techniques based on cryogenically cooled rare-earth-ion-doped crystals have received some interest due to the ability to create high contrast spectral filters using spectral hole burning.[10] In particular, this is highly effective in $Pr^{3+} : Y_2SiO_5$ due to the long spectral hole lifetime.[11] Using spectral hole burning, Li *et al.* demonstrated a 14 dB difference in transmission between the carrier and a single sideband.[12] Also, an order of magnitude improvement in etendue over photorefractive crystals was exhibited.[13] Tay *et al.* realized sensitive detection of ultrasound by utilizing the dispersive properties of spectral holes.[14] The suppression between input pulse and background noise has been further improved by Zhang *et al.* through the use of slow light.[15]

Here, we combine quantum memory techniques with the optical detection of ultrasound, achieving an extremely sensitive level of detection. An effective quantum memory must have both a high storage efficiency and a very low noise level.[10] Both of these properties are also desirable for enabling sensitive detection of ultrasound.

In this work, the atomic frequency comb (AFC)[16,17] is our quantum memory of choice. It was chosen because it can be simply prepared using optical pumping (does not require external electric or magnetic fields), can have high efficiency, and the storage is frequency selective.

The premise behind detection of ultrasound using AFCs is as follows. We generate two AFCs centered at plus and minus the ultrasound frequency on either side of a large spectral pit, itself centered at the frequency of the input laser. As the ultrasonic modulation is applied to the laser beam, the carrier will pass unimpeded through the sample, whereas the (frequency shifted) sidebands will be stored in the AFCs as an echo to be emitted at some later time (defined by the comb parameters). This technique enables a high level of discrimination between the carrier and the sidebands, and as demonstrated this does not depend on the spatial quality of the beam, a necessity for biological imaging applications. We will call this technique the double AFC method of ultrasound detection.

Figure 1 shows the atomic population distribution that is used in the experiments described here. Two AFCs have been created, centered on ± 1.5 MHz, to store the ultrasound. These are separated by a 1.7 MHz wide spectral pit. Note that this pit needs to be wide enough that the entire frequency spectrum of the input pulse can pass through. The finesse of the comb used here is 2 as this gives the highest storage efficiency.[18]

The experimental setup for creating and characterising the AFCs is shown in Fig. 2 and detailed in Ref. 19. The double passed AOM 1 is used to provide frequency agility.

[a)]Electronic mail: jevon.longdell@otago.ac.nz.

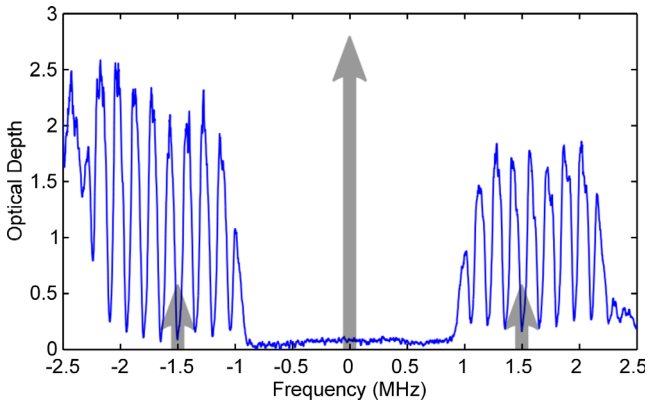

FIG. 1. Distribution of atomic population used in the experiment. It consists of two AFCs centered on the sideband frequencies (± 1.5 MHz) and a broad central hole that allows the carrier beam to pass through without being stored. Here, the AFC peak-to-peak separation is $\Delta = 150$ kHz, the comb finesse is 2, and its optical depth $\alpha L \simeq 2$. The arrows represent the carrier and sideband frequencies of the modulated light. This plot is acquired by scanning the laser frequency slowly using a low light intensity to avoid spectral hole burning (6 MHz sweep in 10 ms, input power $= 660\ \mu$W).

AOMs 2 and 3 are used for creating pulses and provide the net 10.7 MHz frequency shift needed for the heterodyne detection.

There are three parts to the experiment; repumping, comb creation, and echo measurement. Before each experimental run, optical repumping was used to ensure a consistent initial state for praseodymium ions. The repumping was performed using techniques similar to those described in Refs. 20 and 21, resulting in only those ions whose $\pm 3/2(g) - \pm 3/2(e)$ transition is resonant with the laser participating in the experiment. The population distribution shown in Fig. 1 is obtained by applying 2000 repetitions of two pulse trains to the sample to create the AFCs. A series of sweeps over the center frequency is then used to burn the central pit. See the supplemental material for more detail on this step.[19]

The final part of the experiment was the echo sequence: input pulses were applied to the sample and either an echo was detected or the noise level in the detection window was measured (depending on whether the sidebands were on or off, respectively). The input pulse was given a Gaussian temporal distribution, as this maximizes the echo efficiency and also minimizes the width of the pulse in the frequency domain. For each experimental run, the echo sequence was

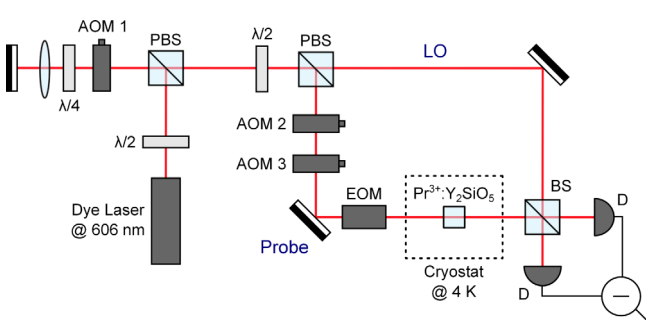

FIG. 2. Experimental setup for creating AFCs and performing balanced heterodyne detection of photon echoes. AOM – acousto-optic modulator, EOM – electro-optic modulator, PBS – polarizing beam splitter, BS – non-polarizing beam splitter, D – detector.

repeated 250 times with no significant degradation in storage efficiency.

A typical echo sequence is shown in Fig. 3(a), both for when the phase sidebands have been applied and when they have not. When the input pulse does not have the phase modulation applied, it passes through the crystal and is not stored, resulting in no echo being formed. However, when the phase modulation is applied to the input, the sidebands are stored in the AFC, resulting in the formation of an echo 6.667 μs $(= 1/\Delta)$ after the input pulse is transmitted. The amplitude of the detected echo experiences a 3 MHz modulation due to interference between the echoes of the two sidebands. Note that when the sidebands are switched on, the transmitted pulse exhibits a 1.5 MHz amplitude modulation. This is due to the atomic population having a non-linear phase response, which turns the phase modulation into amplitude modulation on transmission.

We place an upper bound on the noise present in the echo detection window by measuring the maximum signal in this window when the sidebands are off. Results are presented in Fig. 3(b) as the probe power is varied. Also shown for comparison is the size of the input pulse, and the echo that results when the sidebands are turned on. Each data point is obtained by averaging over 1000 echo traces. Figure 3(b) shows that for a 1 mW input pulse, the peak level of noise in the detection window is 49 dB below the level of the input pulse. Even when the power of the input pulse is reduced by three orders of magnitude and the noise is almost completely due to the local oscillator (LO), 40 dB of discrimination is realized.

The echo efficiency can be calculated from Fig. 3(b). It is necessary to take into account that the sidebands are 8.5 dB smaller than the carrier pulse, and that both sidebands will be contributing to the echo. For a 1 mW input pulse, the echoes are retrieved with an efficiency of 13%.

It is desirable to know whether it is possible to improve the results presented here. Numerical simulations were performed to determine what level of discrimination is theoretically possible. We model our experiment as being a linear system; therefore, the output $(G(\omega))$ can be obtained by multiplying the input $(F(\omega))$ with some transfer function $(T(\omega))$ that describes the frequency response of the system, i.e., $G(\omega) = T(\omega)F(\omega)$. The amplitude response of the system, i.e., the real component of $T(\omega)$, is determined by scanning the laser in frequency as per Fig. 1. The phase response (imaginary component of $T(\omega)$) is then calculated using the Kramers-Kronig relations.[19]

To compare the experimental data with the theoretical prediction, a Gaussian pulse with a FWHM of 1.8 μs is input into the system. The calculated output resulting from this input pulse is plotted in Fig. 4 and compared to a single experimental trace.

Figure 4 shows that the noise level in the experimental data fluctuates, but on average is $\sim$5 dB above that predicted by theory. One explanation for this increase in noise is the non-linear response of the AOMs results in the production of laser pulses that are slightly non-Gaussian in the time domain. It can be seen in Fig. 4 that the shape of the experimental input pulse starts to diverge from that of a true Gaussian at around the -20 dB level.

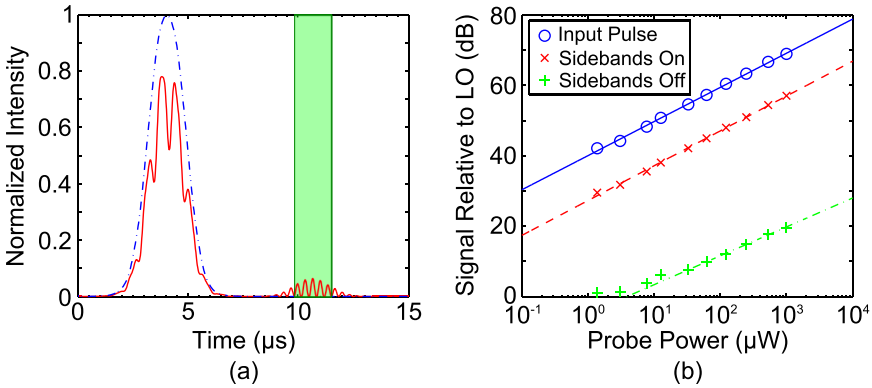

FIG. 3. (a) Example echo sequence with (red solid line) and without (blue dashed line) the phase modulation applied to the input pulse. The green shaded box represents the time window in which the echo intensity (noise level) is measured when the sidebands are on (off). (b) Intensity of the input pulse and the maximum signal in the echo detection window with sidebands on and off, as the power of the input pulse is varied. The signal is measured relative to the local oscillator noise. A linear fit has been made to the three data sets.

For the double AFC technique to have a practical application, it needs to be compatible with biological samples. In order to simulate interactions with biological tissue, the experiment was repeated with a highly scattered laser beam.

A number of modifications were made to the original setup (see Fig. 5(a)). First, the probe beam was scattered by focusing onto an unpolished aluminium surface, collected with a lens, and passed through the sample. The resulting spatial beam distribution is shown in Figure 5(b). Second, given the impossibility of achieving efficient mode matching between the LO and scattered probe beam, the balanced heterodyne detection was replaced with a single photodiode detector. In order to maintain a spatially uniform population distribution throughout the crystal, a non-scattered counter-propagating beam was used to spectrally prepare the sample. Finally, a mechanical shutter was placed in the preparation beam to gate it while the echo sequence was running. AOM2 and AOM3 gate the probe beam during the optical repumping and comb preparation steps.

Figure 5(c) shows that the double AFC technique works even with a highly scattered input beam. Once again, when the sidebands are on, an echo is emitted which is not present when they are off. The echo efficiency is calculated as 10%, so we conclude that the use of the scattered beam does not result in any significant degradation in efficiency.

In this case, the discrimination was 29 dB, limited by the inability of the photodiode based detector to recover quickly from the transmitted carrier. This was verified by moving the laser away from the praseodymium absorption line. Previous studies[15] have been hampered by not achieving the same level of absorption for scattered light as for collimated light. We are hopeful that our technique will not suffer from this problem as light that does not interact with the active atoms for whatever reason, be it polarisation or scattered around the crystal, will appear in the carrier time window and not pollute the sideband time window.

This demonstration was performed at 606 nm using $Pr^{3+}:Y_2SiO_5$, and our results of 49 dB represent a 7 dB improvement over the best discrimination result that has previously been demonstrated.[15] For biomedical imaging, it is problematic that 606 nm sits at the edge of the biological transparency window. A better option in this respect would be, for example, the 790 nm transition in Tm^{3+} doped crystals. The disadvantage of Tm^{3+} is that the primary hole burning mechanism has a relatively short lifetime (10 ms in $Tm^{3+}:YAG$). This has meant that the best discrimination that has been demonstrated is 19 dB.[12] We believe our technique, which does not require high-contrast spectral hole-burning, could be implemented in $Tm^{3+}:YAG$ and could improve this significantly. Indeed AFC memories with similar efficiency to that used here have been demonstrated in $Tm^{3+}:YAG$.[22]

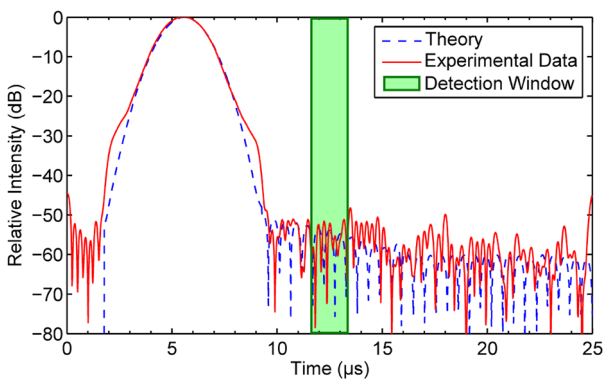

FIG. 4. Comparison of an experimental data trace without the ultrasonic modulation and the results of a theoretical simulation.

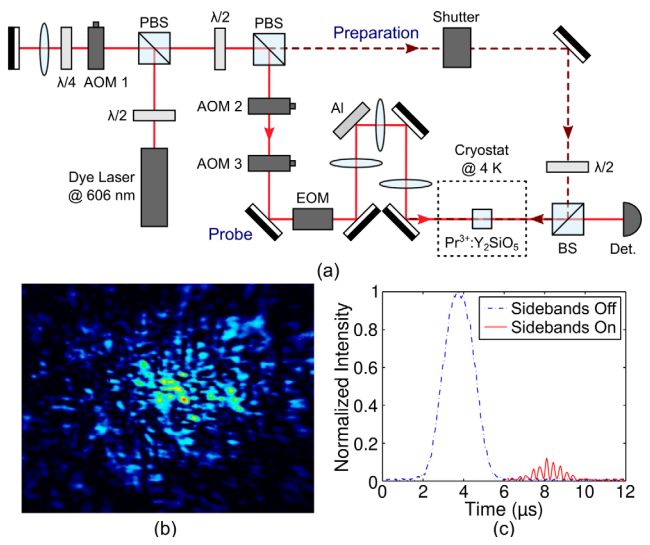

FIG. 5. (a) Experimental setup for detecting echoes using a scattered input beam. Al – piece of unpolished aluminium used to scatter the light. AOM 2 = −80 MHz, AOM 3 = +80 MHz. (b) Spatial distribution of the input beam after scattering. Image taken using a Dataray WinCamD beam profiler. (c) Typical echo sequence showing that the double AFC technique still works with highly scattered light.

In conclusion, we have demonstrated that by using quantum memory techniques, it is possible to detect ultrasound in a manner that is both highly efficient and of low noise. 49 dB of discrimination between the input signal and noise from the carrier was measured, an improvement of 7 dB over previous recorded methods using rare-earth-ion-doped crystals. Because the detection efficiency does not strongly depend on the spatial mode of the laser beam, and because our technique does not require generating optical filters with large optical depth contrast, we consider this technique well suited to the imaging of highly scattering imaging of biological systems.

The authors would like to thank Paul Ewart for his assistance in frequency stabilising the dye laser. This work was supported by the New Zealand Foundation for Research Science and Technology under Contract No. NERF-UOOX0703.

[1]F. A. Marks, H. W. Tomlinson, and G. W. Brooksby, Proc. SPIE **1888**, 500–510 (1993).
[2]R. J. Dewhurst and Q. Shan, Meas. Sci. Technol. **10**(11), R139–R168 (1999).
[3]J.-P. Monchalin, Appl. Phys. Lett. **47**, 14 (1985).
[4]F. Ramaz, B. Forget, M. Atlan, A. C. Boccara, M. Gross, P. Delaye, and G. Roosen, Opt. Express **12**, 5469 (2004).
[5]M. Lesaffre, F. Jean, F. Ramaz, A. C. Boccara, M. Gross, P. Delaye, and G. Roosen, Opt. Express **15**, 1030 (2007).
[6]M. Lesaffre, S. Farahi, M. Gross, P. Delaye, C. Boccara, and F. Ramaz, Opt. Express **17**, 18211 (2009).
[7]T. Bach, M. Jazbinšek, G. Montemezzani, P. Günter, A. A. Grabar, and Y. M. Vysochanskii, J. Opt. Soc. Am. B **24**, 1535 (2007).
[8]M. Jazbinšek, D. Haertle, G. Montemezzani, P. Günter, A. Grabar, I. Stoika, and Y. Vysochanskii, J. Opt. Soc. Am. B **22**, 2459 (2005).
[9]M. Gross, P. Goy, B. C. Forget, M. Atlan, F. Ramaz, A. C. Boccara, and A. K. Dunn, Opt. Lett. **30**, 1357 (2005).
[10]M. P. Hedges, J. J. Longdell, Y. Li, and M. J. Sellars, Nature (London) **465**, 1052 (2010).
[11]B. S. Ham, S. M. Shahriar, and P. R. Hemmer, J. Opt. Soc. Am. B **16**, 801 (1999).
[12]Y. Li, P. Hemmer, C. Kim, H. Zhang, and L. V. Wang, Opt. Express **16**, 14862 (2008).
[13]Y. Li, H. Zhang, C. Kim, K. H. Wagner, P. Hemmer, and L. V. Wang, Appl. Phys. Lett. **93**, 011111 (2008).
[14]J. W. Tay, P. M. Ledingham, and J. J. Longdell, Appl. Opt. **49**, 4331 (2010).
[15]H. Zhang, M. Sabooni, L. Rippe, C. Kim, S. Kröll, L. V. Wang, and P. R. Hemmer, App. Phys. Lett. **100**, 131102 (2012).
[16]H. de Riedmatten, M. Afzelius, M. U. Staudt, C. Simon, and N. Gisin, Nature (London) **456**, 773 (2008).
[17]M. Afzelius, C. Simon, H. de Riedmatten, and N. Gisin, Phys. Rev. A **79**, 052329 (2009).
[18]M. Bonarota, J. Ruggiero, J. L. L. Gouët, and T. Chanelière, Phys. Rev. A **81**, 033803 (2010).
[19]See supplementary material at http://dx.doi.org/10.1063/1.4766341 for a more detailed description of the experimental setup, creating the population distribution, and the Kramers-Kronig theory.
[20]M. Nilsson, L. Rippe, S. Kröll, R. Klieber, and D. Suter, Phys. Rev. B **70**, 214116 (2004).
[21]A. Amari, A. Walther, M. Sabooni, M. Huang, S. Kröll, M. Afzelius, I. Usmani, B. Lauritzen, N. Sangouard, H. de Riedmatten, and N. Gisin, J. Lumin. **130**, 1579 (2010).
[22]T. Chanelière, J. Ruggiero, M. Bonarota, M. Afzelius, and J. Le Gouët, New J. Phys. **12**, 023025 (2010).